Journal of Alloys and Compounds 509 (2011) 1958–1963

Contents lists available at ScienceDirect

Journal of Alloys and Compounds

journal homepage: www.elsevier.com/locate/jallcom

Effects of titanium addition on mechanical and corrosion behaviours of AZ91 magnesium alloy

S. Candan[a], M. Unal[b], E. Koc[b], Y. Turen[b], E. Candan[a,*]

[a] Department of Mechanical and Manufacturing Engineering, Bilecik University, 11210 Bilecik, Turkey
[b] Department of Metals, Karabuk University, 78200 Karabuk, Turkey

ARTICLE INFO

Article history:
Received 9 November 2009
Received in revised form 10 October 2010
Accepted 21 October 2010
Available online 30 October 2010

Keywords:
Magnesium
AZ91 alloy
Mechanical properties
Corrosion

ABSTRACT

The mechanical properties and corrosion behaviour of AZ91 magnesium alloy containing 0.2–0.5 wt.% Ti were investigated in this study. Results demonstrate that the enhancement of the ultimate tensile strength by 18% and yield strength by 47% can be achieved by Ti addition. The corrosion behaviour was evaluated by immersion tests and potentiodynamic polarisation measurements in 3.5% NaCl solution. The results from the immersion tests and potentiodynamic polarisation measurements showed that the corrosion resistance of AZ91 alloy increased progressively with the increase of the Ti content of the alloy. Compared to AZ91 alloy, 0.5Ti addition increased the corrosion resistance by up to 45 fold. The mechanism of property enhancement is ascribed to both the suppression of partially divorced β-$Mg_{17}Al_{12}$ eutectics and an increased Al content in α-Mg solid solution by Ti addition in AZ91 alloy.

1. Introduction

Magnesium and magnesium alloys are used in a wide variety of structural applications including automotive, aerospace, materials-handling, portable microelectronics and telecommunication industries due to their low density. Among the magnesium alloys, AZ91 magnesium alloy is one of the most successfully used commercial alloy, which contains 9Al–1Zn and a small quantity of Mn. However, the application of the AZ91 magnesium alloy is still limited owing to its limited strength and relatively lower corrosion resistance as compared to the aluminium alloys [1]. In order to enhance its tensile strength and corrosion resistance, minor alloying is extensively employed to improve microstructure of the AZ91magnesium alloy [2–22].

Ca is an effective way to improve the mechanical properties of AZ91 alloys at elevated temperatures [7–11]. Other elements such as Sb, Bi and Pb to AZ91 alloy could also increase the tensile strength and creep resistance significantly [9,10,12–14]. A recent study [15] showed that the presence of Sn contributed to the room and the elevated temperature strength of magnesium alloy attributed to the formation of dispersed short rod-like Mg_2Sn phases. The addition of B in the form of Al-4B master alloy significantly refines the grain size of AZ91 leading to an improvement in the mechanical properties [16]. The beneficial effects of rare-earth (RE) on mechanical properties including strength and creep resistance of AZ91 alloys also have been reported [7,8,11,17–19].

The corrosion resistance of AZ91 relatively is higher than that of pure magnesium largely owing to the substantial alloying addition which constitutes approximately 10 wt.% of the alloy. However, the heterogeneous microstructure of AZ91 also stimulates a localised corrosion morphology that is dictated by the distribution of the β-$Mg_{17}Al_{12}$ intermetallic phases in the matrix [1]. Although, there have been several emerging studies reported on the influence of various minor alloying additions to the microstructure and mechanical properties of AZ91, knowledge of the influence of these elements on the corrosion resistance of Mg alloys is relatively lacking. Addition of Sb or Bi reduce the corrosion resistance of AZ91 alloy due to formation of Mg_3Sb_2 or Mg_3Bi_2 phases which act as effective cathode to the α-Mg matrix [9]. Combination of Sb and Bi to the AZ91 alloy also resulted in significant decrease in corrosion resistance [9]. However, combined addition of Sb and Si showed increment in corrosion resistance which was reported to be due to the formation of fine polygonal shaped Mg_2Si phases inhibiting the corrosion more effectively compared to its Chinese script form [20]. With the addition of Ca to AZ91, corrosion resistance increased due to the formation of the reticular Al_2Ca phase, which acted as an effective barrier against corrosion [8] or showed no detrimental effect [9]. Improved corrosion behaviours of AZ91 alloys also have been reported with Ce addition [8,18,21]. The addition of Ce to AZ91D alloy formed the more continuous β phase, which acts as a corrosion barrier [18] while another study [21] reported that Ce in AZ91 alloy can reduce the grain size, impede the formation of oxide, and thereby improves the corrosion performance. Zang et al. [19] found that the addition of Yttrium was of significant effect on the improving of the corrosion resistance with respect to the grain refinement. The improvement of corrosion resistance

* Corresponding author. Tel.: +90 0228 2160101; fax: +90 0228 2160287.
E-mail address: ecandan@yahoo.com (E. Candan).

0925-8388/$ – see front matter © 2010 Elsevier B.V. All rights reserved.
doi:10.1016/j.jallcom.2010.10.100

in Ho-containing Mg–9Al–Ho alloys was reported to be due to the less cathodic Ho-containing phases and the corrosion product film on the surface restraining further corrosion [22]. Literature above reveals that improved corrosion behaviour of AZ91 alloy could be achieved by the formation of favourable intermetallics, modification of β-$Mg_{17}Al_{12}$ intermetallics or modification of oxide layer on the surface. However, our previous work showed that Pb addition suppresses the formation of intermetallics which led to improved corrosion resistance as well as mechanical properties in AZ91 alloy [14]. In the literature [23], the effect of Ti addition on the corrosion behaviour of AZ91 alloy is scarce and no systematic study has been reported on its effect on mechanical and corrosion behaviours of AZ91 alloy. Therefore, the aim of this work was to investigate the effect of minor Ti alloying additions (0.2–0.5 wt.% Ti) to AZ91 alloy on its mechanical properties and corrosion resistance.

2. Experimental procedures

Mg, Al and Zn ingots with the minimum purity of 99.90% and Al–Ti alloy (5.0 wt.% Ti) were purchased from Karasu Metal Co., Turkey. Master alloys were prepared by melting pure Mg together with pure Al and Al–Ti alloy in a graphite crucible under Ar gas atmosphere at 750 °C and cast as ingot form. Zn addition was carried out 1 min before the casting to avoid loss of Zn due to vaporisation. The master alloy was then remelted and cast into a cast iron mould (preheated to 250 °C) having a 30 mm diameter and a 170 mm length under protective SF_6 gas. The alloy specimens were used in as-cast form. The compositions of the studied alloys are listed in Table 1, obtained by using Spectrolab M8 Optical Emission Spectrometry (OES). The hardness values were determined by the Vickers hardness test with a load of 50 N. At least ten successive hardness measurements were made on each sample. The tensile test samples had a diameter of 8 mm and a length of 40 mm. The tensile tests were performed (ASTM E 8M-99) with a crosshead speed of 0.8 mm min^{-1} at room temperature. Each data represents at least average of five samples in tensile tests. X-Ray Diffraction (XRD) analysis (Philips RV 3710X-Ray Diffractometer) was carried out under CuKα radiation with the incidence beam angle of 2°. The diffraction angle range was between 20° and 100° with a step increment of 0.02° and a count time of 1 s. Microstructural evaluations were carried out by optical light microscopy and JEOL-JSM 6500 scanning electron microscopy (SEM). The samples were etched in 1 ml HNO_3, 24 ml and 75 ml ethylene glycol solution.

Samples having 10 mm in length and 25 mm in diameter were machined and subsequently ground with 220, 400 and 600 grit emery papers followed by polishing with 1 μm diamond paste for the immersion tests and microstructural evaluations. After through cleaning well with alcohol the samples were weighed and then immersed in 3.5% NaCl solution for 72 h for immersion tests. After the immersion tests, the samples were cleaned with a solution containing 200 g/l CrO_3 + 19 g/l $AgNO_3$ for 10 min to remove the corrosion products. Finally, they were cleaned with distilled water, dried and weighed. The corrosion loss of the samples were then normalized in the unit of mg/cm^2 d by considering the total surface area of the samples and referred to corrosion loss thereafter. For the potentiodynamic polarisation measurements, machined samples of 15 mm in length and 10 mm in diameter were connected to copper wire and embedded in an epoxy resin holder. The surfaces were then abraded on 600 mesh emery paper, mechanically polished with 1 μm diamond paste and washed and ultrasonically rinsed in distilled water. The potentiodynamic curves were performed by means of a Gamry model PC4/300 mA potentiostat/galvanostat controlled by a computer with DC105 corrosion analysis software. The embedded specimens in epoxy resin were utilized as working electrodes. A carbon rod (6 mm in diam.) and a saturated calomel electrode (SCE) were used as a counter electrode and reference electrode respectively. Experiments were performed at room temperature in a glass cell containing 3.5% NaCl solution. Each polarisation experiment was carried out holding the electrode for 1 h at open circuit potential (E_o) to allow steady-state to be achieved. Potentiodynamic polarisation curves were generated by sweeping the potential from cathodic to anodic direction at a scan rate of 1 mV s^{-1}, starting from −2.00 up to −0.10 V. Each data point for both immersion and potentiodynamic polarisation tests represents at least average of 3 different measurements.

Table 1
Chemical compositions of the alloys studied.

Alloy	Analyzed composition (wt.%)							
	Al	Zn	Mn	Ti	Cu	Fe	Ni	Si
AZ91	9.11	0.97	0.15	–	0.007	0.09	0.002	0.08
AZ91 + 0.2Ti	8.78	0.94	0.12	0.17	0.009	0.06	0.001	0.03
AZ91 + 0.5Ti	8.93	0.95	0.10	0.54	0.008	0.01	0.001	0.03

3. Results and discussion

The XRD analysis indicated that both AZ91 and AZ91 + 0.5Ti alloys mainly consist of α-Mg solid solution and the compound of intermetallic β-$Mg_{17}Al_{12}$ phases (Fig. 1). In Fig. 2a–c, optical micrograph images of AZ91, AZ91 + 0.2Ti and AZ91 + 0.5Ti alloys are illustrated respectively. The microstructure of AZ91 alloy consisted of primary α-Mg and β-$Mg_{17}Al_{12}$ phases (arranged along the α-Mg matrix grain boundary) which is consistent with the published literature [20]. It was observed that rosette-like equiaxed α-Mg grains had coarsened and the morphology of the β-$Mg_{17}Al_{12}$ phases had been altered by Ti addition (Fig. 1c). Net-like intermetallic phases had been progressively reduced with the increasing Ti content (Fig. 1a–c). According to the Mg–Al equilibrium phase diagram, the eutectic $Mg_{17}Al_{12}$ is expected to appear when the aluminium content reaches ~13 wt.%. However, the eutectic phase appears in alloys containing as little as 2 wt.% Al for nonequilibrium cooling conditions normally encountered in castings [24]. Depending on alloying additions and/or solidification conditions fully divorced, partially divorced or lamellar eutectic morphologies can be formed in magnesium alloys [25,26].

Further observations from backscattered SEM images in Fig. 3a and b revealed that the β eutectics appeared in bright contrast in the morphology of divorced, partially divorced and lamellar in accordance with the microstructural evaluation of AZ91 alloy in the literature [20,25–28]. Generally, the lamellar type eutectics were located adjacent to partially divorced β in AZ91 alloy as shown in Fig. 3a. Some islands can be observed in β-$Mg_{17}Al_{12}$ phases under high magnification (Fig. 3a) in the AZ91 alloy indicating that the eutectic is partially divorced. Meanwhile, no islands can be seen in the refined β-$Mg_{17}Al_{12}$ phases (Fig. 3b) and that is evidence of the fully divorced eutectic by 0.5Ti addition. The eutectic morphologies of magnesium casting alloys and the variation of these morphologies have been explained in Ref. [26]. The predominance of fully or partially divorced morphologies is mainly depended upon the solidification rate, the volume fraction of the aluminium content and the primary dendrites in AZ series Mg alloys. It has been established that the probability of forming a fully divorced eutectic can be increased by the addition of small amounts of Zn to Mg–Al alloys. Due to the high segregation tendency of Zn during cooling and

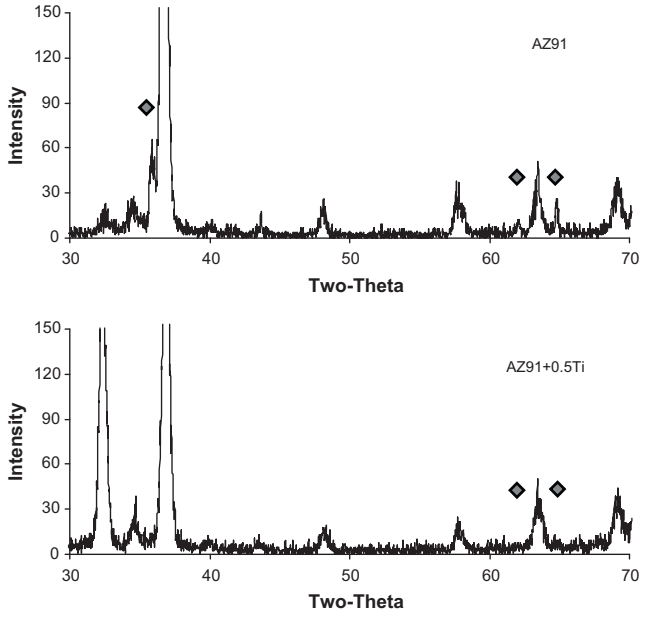

Fig. 1. XRD patterns of AZ91 and AZ91 + 0.5Ti alloys. The peaks marked with a diamond are from β ($Mg_{17}Al_{12}$) and all other peaks are from α-Mg.

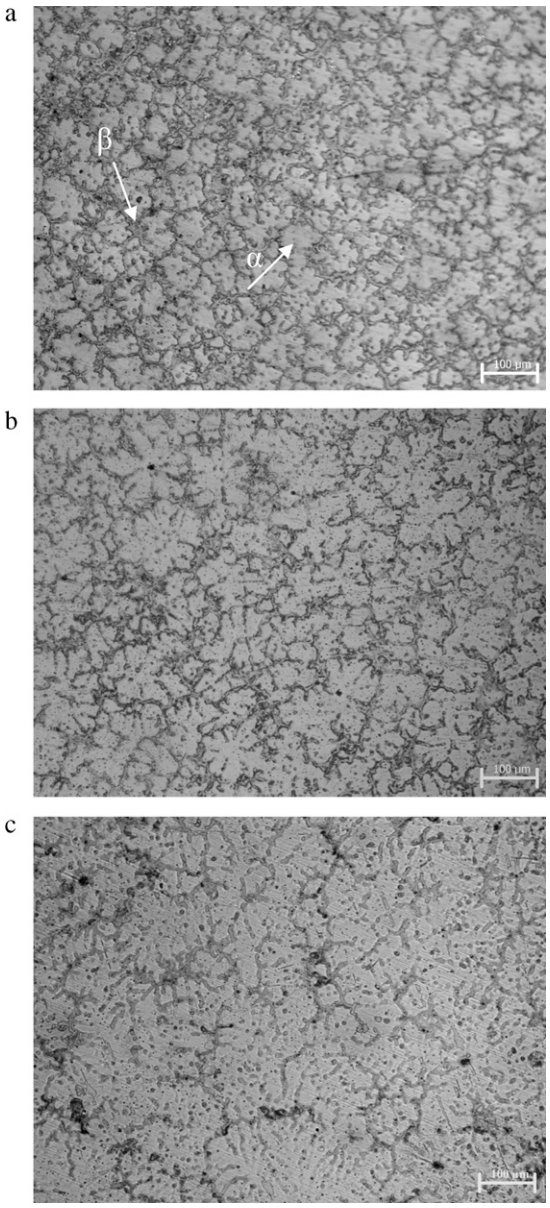

Fig. 2. Optical microstructure of (a) AZ91, (b) AZ91 + 0.2Ti and (c) AZ91 + 0.5Ti alloys.

the degree of constitutional undercooling ahead of the solid-liquid interface during the early stages, there is a considerable increase in primary dendrite growth. This reduces the size of the interdendritic space, which in turn favours the fully divorced β eutectic [25,26]. Generally, fully divorced morphologies are formed in die-casting or lower Al contents, whereas partially divorced morphologies are more likely at lower cooling rates and higher Al contents. Lamellar eutectic occurs from supersaturated α-Mg solid solution (adjacent to divorced β eutectics) which decomposes into lamellar β and solute α-Mg through solid state transformation [29,30].

The effects of Ti on eutectic morphology of AZ series Mg alloys seem not to be reported. Mg and Ti have not been found to form intermetallic compounds and they have very little (0.2 wt.% max.) mutual solubility [31]. EDS analysis revealed that mean Al amounts of α-Mg matrix in AZ91, AZ91 + 0.2Ti and AZ91 + 0.5Ti alloy were around 3.2, 4.7 and 6.1 respectively. Evidently, the Al content of α-Mg matrix increased nearly twofold (from 3.2 to 6.1 wt.% Al) with 0.5Ti additions to AZ91 alloy. It is believed that Ti addition might have effectively reduced the diffusion of Al in Mg matrix, which is the principal phenomenon for the formation and growth of precipitation. Thus, the suppression of the partially divorced and lamellar eutectics was attributed to increased solubility of Al in α-Mg. As discussed earlier, fully divorced morphologies are formed in faster solidification rates or lower Al contents. An increased Al content in α-Mg reduces Al segregation at the end of the dendrites promoting the formation of fully divorced eutectics.

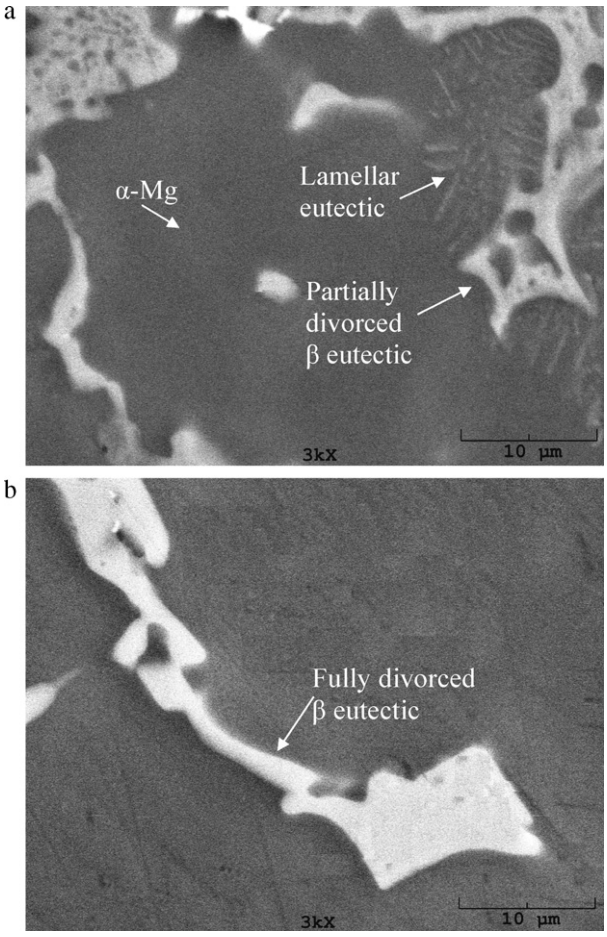

Fig. 3. SEM morphology of the secondary phases in (a) AZ91 and (b) AZ91 + 0.5Ti alloy.

In addition, a different phase (unlike common phases in AZ series) with a mixture of fine particles and needles scarcely dispersed in the grains and boundaries was observed in the microstructure of AZ91 + 0.5Ti alloy (Fig. 4). The appearance of the new phase was similar to partially divorced β eutectics and was difficult to distinguish without etching since they contained α-Mg islands in their structure and they were scarcely dispersed in the microstructure. As illustrated in Fig. 4, the new phase mainly consisted of Ti, Fe, Si as well as Mg and Al obtained by EDS analysis. The amounts of Ti, Fe and Si in the new phases varied between 10–25, 7–14 and 3–9 wt.% respectively. Some of them also contained oxygen which varied from 0 to 22%. Since the solid solubility of Ti in Mg is 0.2 wt.% [31], the excess Ti in AZ91 + 0.5Ti alloy probably combined with Fe, Si and in some cases with addition of oxygen. Since the melting was carried out under inert atmosphere, the source of oxygen could be from the atmosphere during pouring to permanent mould. Formation and kinetics of the new phase is a subject for further study and is an ongoing work. However, the preliminary observations indicated that the presence of excess Ti beyond the solubility limit in α-Mg, scavenged Fe and Si trace elements by forming the new phase.

Figs. 5–7 show the dependence of the ultimate tensile strength (UTS), yield strength (YS), elongation (EL) and hardness (HV) of

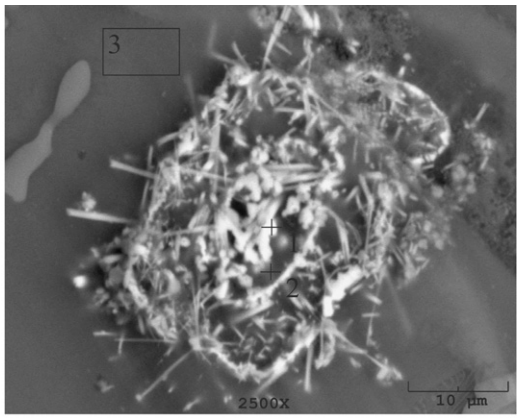

Area/Element	O	Mg	Al	Si	Ti	Mn	Fe
1	20.8	20.7	19.4	8.9	16.7	2.5	10.9
2	10.6	53.5	11.0	3.5	13.6	1.7	5.9
3	-	91.4	8.3	-	-	-	-

Fig. 4. SEM morphology of the additional phase appeared in the microstructure of AZ91 + 0.5Ti alloy.

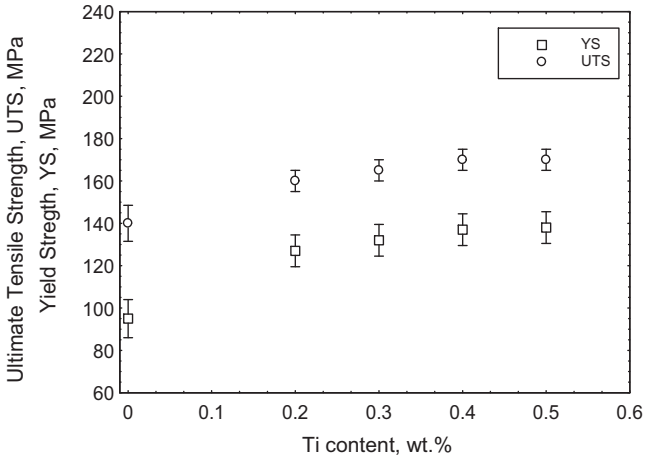

Fig. 5. Ultimate tensile strength (UTS) and yield strength (YS) of AZ91 alloy as a function of its Ti content.

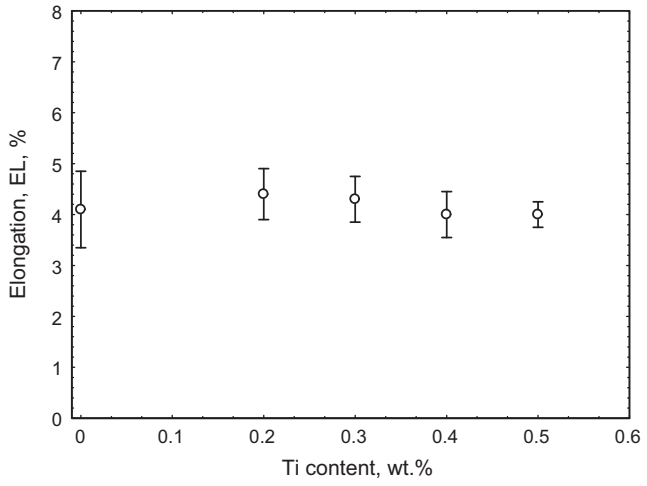

Fig. 6. Elongation (EL) of AZ91 alloy as a function of its Ti content.

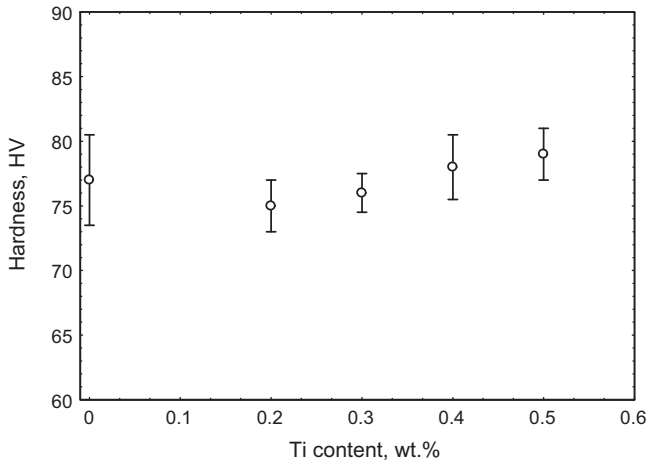

Fig. 7. Hardness (HV) of AZ91 alloy as a function of its Ti content.

AZ91 alloy on its Ti content respectively. Evidently, UTS and YS increase with the increase of Ti content of AZ91 alloy (Fig. 5). Especially interesting is that the UTS and YS of AZ91 alloy increased from 144 to ~170 MPa (i.e. an 18% increase) and from 95 to ~140 MPa (i.e. a 47% increase) by 0.5Ti addition respectively. Elongation, EL and HV were not altered notably by Ti addition as shown in Figs. 6 and 7. The presence of β intermetallics means that there is a continuous easy crack path of brittle phase along the α-Mg grain boundary. The alloy is expected to exhibit low ductility because the net-like brittle intermetallic phase at the α-Mg grain boundary easily breaks up and causes cracking during plastic deformation. As a consequence, there is a resulting low elongation and concomitant low strength for the AZ91 alloy yielding ~144 MPa UTS and ~4% EL. These results are partially in accordance with the literature [8,28]. Zhao et al. [28] reported 126 MPa UTS and 3.3% EL for AZ91 alloy whereas Wu et al. [8] reported 145 MPa UTS and 1.5% EL. The deviations from the reported results [8,28] may be due to the production conditions of the alloy (i.e. casting temperature, solidification condition, composition, etc.) which may alter the amount, size and morphology of the intermetallics. For example, Zhao et al. [28] used the samples from ingots, whereas in the present study molten alloy was cast into a 30 mm diameter cast iron chill. The increase in the UTS and YS by Ti addition up to 0.5Ti is attributed to reduction of net-like brittle β phases in the grain boundaries, changes in the morphology of β phase (predominantly divorced eutectics rather than partially divorced or lamellar type) and solid solution strengthening due to an increase in Al content (see Table 1). Refinement of the interface between α-Mg and β phase by Ti addition (i.e. suppression of partially divorced and lamellar β phase, Fig. 1a and b) should eliminate uneven crack initiation sites during tensile tests. This is further supported by Fig. 6 which demonstrates that scattering in EL was considerably reduced in AZ91 + 0.5Ti alloy as compared to AZ91 alloy. Thus the influence of Ti addition on mechanical properties is attributed to the suppression of the net-like intermetallics which results in no continuous crack path through the grain boundaries. Furthermore, Dobrzanski et al. [32] reported that the dissolution of intermetallics by heat treatment resulted in supersaturated solid solution α-Mg with visible dislocation ranges and β phase in the form of precipitations with different crystallographic orientations partly coherent with the matrix grains. In the present work, it is believed that Ti addition may also cause a similar effect by suppressing partially divorced and lamellar intermetallics leading to formation of finer fully divorced β precipitates distributed throughout the matrix, which could block the movement of dislocations by Orowan looping. Increased Al concentration should also result in solute solution hardening in the α-Mg matrix.

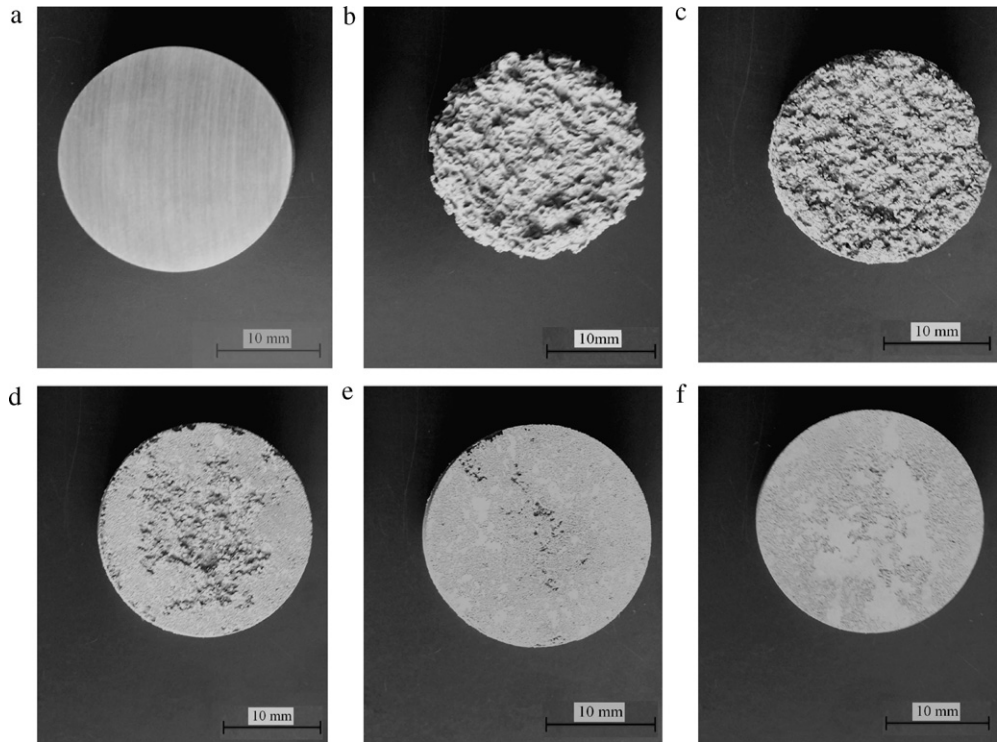

Fig. 8. Macroscopical pictures of (a) AZ91 alloy before corrosion, (b) AZ91, (c) AZ91 + 0.2Ti, (d) AZ91 + 0.3Ti, (e) AZ91 + 0.4Ti and (f) AZ91 + 0.5Ti alloy exposed to 3.5%NaCl for 72 h.

Fig. 8 illustrates macroscopical pictures of AZ91 alloy before and after immersion tests as a function of its Ti content. It is obvious that the whole surface suffers from heavy corrosion while its corrosion resistance increased significantly with increasing Ti content. Fig. 9 presents the results obtained from the immersion tests of corrosion loss of the corroded AZ91 alloys as a function of its Ti content. The mass loss decreased from 77 mg/cm^2 d to 1.7 mg/cm^2 d as 0.5Ti was added to AZ91 alloy, yielding around 45 times higher corrosion resistance. Compared to published works [19,20,30], the heavier corrosion loss in AZ91 alloy was attributed to a higher impurity (i.e. Fe) level of Mg used in this study. For example, the Fe content in the work of Zang et al. [19] was 0.024 wt.% whereas it was 0.090 wt.% in the present work, corresponding to nearly four times higher Fe. Fig. 10 shows potentiodynamic polarisation curves as a function of Ti content indicating that increasing Ti addition improves corrosion resistance (curves for 0.3 and 0.4Ti were not included in the figure for clarity but their curves sit between 0.2 and 0.5Ti). The results in Fig. 10 are very much in line with the immersion tests. Corrosion potential (E_{corr}), and corrosion current density (I_{corr}), obtained from their polarisation curves are also given in Fig. 10. For example, the 0.5Ti addition resulted in E_{corr} shifting negatively by 159 mV and I_{corr} decreasing by 110 μA/cm^2. A promising alloying addition does not necessarily raise the E_{corr} of the alloy to a more noble potential but rather shows a lower corrosion rate [23]. In this study, Ti additions which improve the overall corrosion resistance does in fact lower the E_{corr} (more active) while decreasing the corrosion rate in accordance with the work of Südholz et al. [23]. Fig. 10 reveals that the Ti alloying additions decrease the rate of cathodic

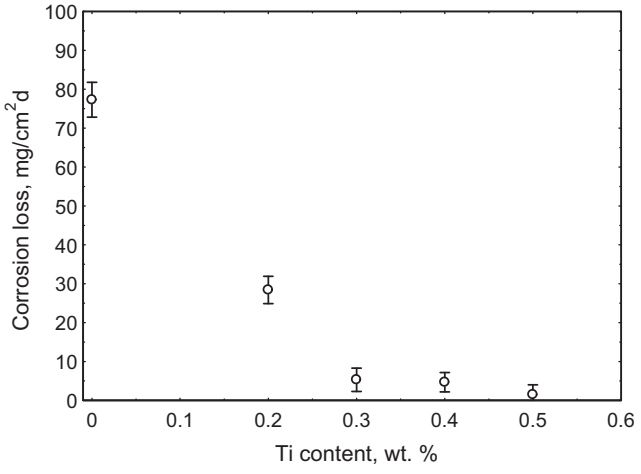

Fig. 9. Corrosion loss of the corroded AZ91 alloys as a function of Ti content from the immersion tests.

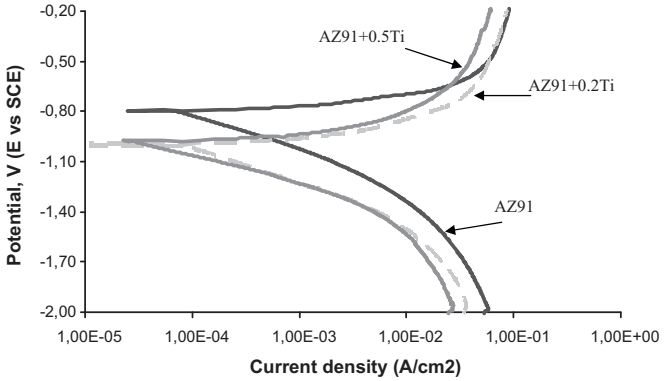

Alloy	AZ91	AZ91+ 0.2Ti	AZ91+ 0.3Ti	AZ91+ 0.4Ti	AZ91 + 0.5Ti
Ecorr, (mV)	-821	-990	-999	-996	-980
Icorr, (μA/cm^2)	153.0	119	103	86	43

Fig. 10. Potentiodynamic polarisation curves for AZ91, AZ91 + 0.2Ti and AZ91 + 0.5Ti alloy in 3.5% NaCl environment with corresponding E_{corr} and I_{corr} values.

reaction kinetics compared to AZ91 alloy. Based on galvanic corrosion principles, the total surface area of cathode (intermetallics) in relation to the surface area of the anode (α-Mg) governs the galvanic corrosion. Zhao et al. [30] reported that β eutectics in AZ91 alloy can cause micro-galvanic acceleration of corrosion. Therefore, it is expected that a reduced amount of intermetallics (cathode) and a refined interface in Ti added alloys should reduce the corrosion rate due to reduced micro-galvanic sites. It should also be noted that the transformation from partially divorced and lamellar β eutectics to fully divorced β eutectics could contribute to an additional reduction in micro-galvanic sites because partially divorced β eutectics contain α-Mg islands (as discussed earlier). An increased Al content, as a solid solution in Mg, may also have an additional beneficial effect on corrosion resistance in accordance with the reported works [33]. Its effect was explained as a formation of stable oxide film on the surface [29,30,33]. As discussed earlier, the excess Ti above solid solubility (>0.2 wt.% Ti) in 0.5Ti-added alloys had combined with Fe and Si (Fig. 4). This may contribute to the corrosion resistance by scavenging Fe and Si that are detrimental to corrosion resistance of Mg [31,33]. In addition, the presence of Ti in the α-Mg matrix as solid solution may also have a positive effect in a way similar to that of Al in solid solution.

4. Conclusions

Based on the above observations, following conclusions can be drawn on the role of Ti on the mechanical and corrosion properties of AZ91 alloy:

- Small amounts of Ti addition to AZ91 alloy resulted in considerable grain refinement of β eutectics. Net-like partially divorced β eutectics were progressively reduced with increasing Ti content.
- The ultimate tensile and yield strength of 0.5Ti added to AZ91 alloy increased by 18% and by 47% respectively, attributed to the reduction of brittle netlike partially divorced β eutectics.
- The 0.5Ti addition to AZ91 alloy resulted in 45 fold improvements in corrosion resistance. This significant improvement can be attributed to the following four factors: (i) the microstructural change from partially divorced eutectic to fully divorced eutectics, (ii) the increased Al solid solution content of α-Mg, (iii) the presence of Ti in solid solution and (iv) the scavenging of detrimental Fe and Si impurities by the addition of Ti above the solid solubility limit of Mg.

References

[1] K.U. Kainer, Magnesium Alloys and Technology, Wiley-VCH, Verlag GmbH & Co. KGaA, 2003.
[2] M.O. Pekguleryuz, A.A. Kaya, Adv. Eng. Mater., DGM 5 (2004) 1–10.
[3] N. Balasubramani, A. Srinivasan, U.T.S. Pillai, B.C. Pai, Mater. Sci. Eng. A 457 (2007) 275–281.
[4] T. Zhu, Z.W. Chen, W. Gao, J. Alloys Compd. 501 (2010) 291–296.
[5] A. Srinivasan, U.T.S. Pillai, B.C. Pai, Mater. Sci. Eng. A 527 (2010) 6543–6550.
[6] S.F. Liu, L.Y. Liu, L.G. Kang, J. Alloys Compd. 450 (2008) 546–550.
[7] D. Wenwen, S. Yangshan, M. Xuegang, X. Feng, Z. Min, W. Dengyun, Mater. Sci. Eng. A 356 (2003) 1–7.
[8] G. Wu, Y. Fan, H. Gao, C. Zhai, Y.P. Zhu, Mater. Sci. Eng. A 408 (2005) 255–263.
[9] W. Zhou, N.N. Aung, Y. Sun, Corros. Sci. 51 (2009) 403–408.
[10] Y. Guangyin, S. Yangshan, D. Wenjiang, Mater. Sci. Eng. A 308 (2001) 38–44.
[11] F. Wang, Y. Wang, P. Mao, B. Lu, Q. Guo, Trans. Nonferrous Met. Soc. 20 (2010) 311–317.
[12] Y. Guangyin, S. Yangshan, D. Wenjiang, Scr. Mater. 43 (2000) 1009–1013.
[13] A. Srinivasan, J. Swaminathan, M.K. Gunjan, U.T.S. Pillai, B.C. Pai, Mater. Sci. Eng. A 527 (2010) 1395–1403.
[14] S. Candan, M. Unal, M. Turkmen, E. Koc, Y. Turen, E. Candan, Mater. Sci. Eng. A 501 (2009) 115–118.
[15] B.H. Kim, S.W. Lee, Y.H. Park, I.M. Park, J. Alloys Compd. 493 (2010) 502–506.
[16] M. Suresh, A. Srinivasan, K.R. Ravi, U.T.S. Pillai, B.C. Pai, Mater. Sci. Eng. A 525 (2009) 207–210.
[17] F. Yu, W. Guohua, G. Hongtao, L. Guanqun, Z. Chunquan, J. Mater. Sci. 41 (2006) 5409–5416.
[18] F. Yu, W. Guohua, Z. Chunquan, Mater. Sci. Eng. A 433 (2006) 208–215.
[19] J. Zang, X. Niu, X. Qiu, K. Liu, C. Nan, D. Tang, J. Meng, J. Alloys Compd. 471 (2009) 322–330.
[20] Srinivasan, S. Ningshen, U. Kamachi Mudali, U.T.S. Pillai, B.C. Pai, Intermetallics 15 (2007) 1511–1517.
[21] Y. Liu, Q. Wang, Y. Song, D. Zhang, S. Yu, X. Zhu, J. Alloys Compd. 473 (2009) 550–556.
[22] X. Zhou, Y. Huang, Z. Wei, Q. Chen, F. Gan, Corros. Sci. 48 (2006) 4223–4233.
[23] A.D. Südholz, N. Birbilis, C.J. Bettles, M.A. Gibson, J. Alloys Compd. 471 (2009) 109–115.
[24] Y. Cheng, T. Qin, H. Wang, Z. Zhang, Trans. Nonferrous Met. Soc., China 19 (2009) 517–524.
[25] M.D. Nave, A.K. Dahle, D.H. St. John, in: I. Howard Kaplan (Ed.), Proceedings of the Magnesium Technology (Tennessee 2000) pp. 243–250, 2000.
[26] A.K. Dahle, Y.C. Lee, M.D. Nave, P.L. Schaffer, D.H. StJohn, J. Light Met. 1 (2001) 61–72.
[27] M. Anık, E. Korpe, Surf. Coat. Technol. 201 (2007) 4702–4710.
[28] M.C. Zhao, Y.L. Deng, X.M. Zhang, Scr. Mater. 58 (2008) 560–563.
[29] G. Song, A. Atrens, M. Dargusch, Corros. Sci. 41 (1999) 249–273.
[30] M.C. Zhao, M. Liu, G. Song, A. Atrens, Corros. Sci. 48 (2008) 1939–1953.
[31] I.J. Polmear, in: M. Avedisian, H. Baker (Eds.), Magnesium and Magnesium Alloys, ASM Speciality Handbook, 1999.
[32] L.A. Dobrzanski, T. Tanski, L. Cizek, Z. Brytan, J. Mater. Proc. Technol. 192–193 (2007) 567–574.
[33] G. Song, J. Corros. Sci. Eng. 6 C104 (2003) 1–19.